J. Fluid Mech. (1992), *vol.* 243, *pp.* 51–72
Printed in Great Britain

On the stability of weakly nonlinear short waves on finite-amplitude long gravity waves

By JUN ZHANG[1] AND W. K. MELVILLE[2]†

[1] Ocean Engineering Program, Department of Civil Engineering, Texas A & M University, College Station, TX 77843, USA

[2] R. M. Parsons Laboratory, Massachusetts Institute of Technology, Cambridge, MA 02139, USA

(Received 14 February 1991 and in revised form 4 March 1992)

The modulated nonlinear Schrödinger equation (Zhang & Melville 1990), describing the evolution of a weakly nonlinear short-gravity-wave train riding on a longer finite-amplitude gravity-wave train is used to study the stability of steady envelope solutions of the short-wave train. The formulation of the stability problem reduces to the solution of a pair of coupled equations for the disturbance amplitude and (relative) phase. Approximate analytical solutions and numerical solutions show that the conventional sideband (Benjamin–Feir) instability is just the first in a series of resonantly unstable regions which increase in number with increasing perturbation wavenumber. The first of these new instabilities is the result of a quintet resonance between four short waves and one long wave. Subsequent unstable regions correspond to sextet or higher-order resonances. The results presented here suggest that steady envelope solutions for unforced irrotational short waves on longer irrotational gravity waves may be unstable for a wide range of conditions.

1. Introduction

In a recent paper we derived a nonlinear Schrödinger equation describing the evolution of weakly nonlinear short waves riding on a longer finite-amplitude gravity wave (Zhang & Melville 1990; hereinafter referred to as ZM). That work was motivated by issues of air–sea interaction and remote sensing described in the Introduction of ZM. We found steady solutions (relative to the long-wave profile) of the short-wave envelope for wavelength ratios of $O(10^{-2})$. Recently Zhang (1990, 1991) rederived the modulated nonlinear Schrödinger equation using a variational principle based on the phase-averaged Lagrangian (Whitham 1965, 1974), and extended the formulation to include larger wavelength ratios of $O(10^{-1})$. Comparisons of the steady solutions with those of Longuet-Higgins (1987) for linear short waves showed an increase in the modulation of the short wavelength with increasing short-wave steepness. However, at small wavelength ratios the modulation of the short-wave amplitude decreases with increasing short-wave steepness, but may increase at larger wavelength ratios. Therefore we expect stronger wave steepness modulation for short waves on relatively long waves.

Many of the models of long-wave–short-wave modulation assume (implicitly if not explicitly) that such steady envelope solutions may be realized and that they are

† Present address: Scripps Institution of Oceanography, University of California, San Diego, La Jolla, CA 92093-0213, USA.

stable. As indicated in ZM, one motivation for deriving the modulated nonlinear Schrödinger equation was to investigate the stability of the steady envelope solutions. It is well known that in the absence of any longer wave a uniform weakly nonlinear gravity-wave train is unstable to sideband disturbances (Benjamin & Feir, 1967). At larger slopes (outside the range of validity of the nonlinear Schrödinger equation), other two- and three-dimensional instabilities may occur (see MacKay & Saffman 1986, and references therein). Thus in this case we expect that the Benjamin–Feir instability will be affected by the longer wave. Further, the long-wave–short-wave system may be viewed as a system of coupled oscillators, as has been modelled by Henyey *et al.* (1988). It is well known that such systems may have multiple unstable regions.

Owing to the modulation by the long wave, both the short-wave steepness and perturbation wavenumber change along the wave, but at quite different rates. Thus the ratio of the nonlinearity to dispersion terms in the modulated Schrödinger equation changes along the long wave. Consequently, the relative phase between a pair of sideband resonant disturbances must change accordingly, whereas in the absence of the long wave, the sideband instability is characterized by a constant relative phase. Therefore, the resonant growth rate of disturbances along the long wave depends on the short-wave steepness as well as the relative phase.

For the sideband instability with a small perturbation wavenumber (corresponding to Benjamin–Feir instability), the relative phase is modulated about a constant value. With an increase in the perturbation wavenumber, the relative phase may change monotonically along the long wave, and for certain ranges of the wavenumber it may change by $2N\pi$ (N an integer) in one long wavelength, leading to a periodic resonant growth rate, changing sign $2N$ times in one long wavelength. However, the net growth over one long wavelength may still be significant owing to the modulation by the long wave. For example, if the magnitude of the resonant growth rate at the crest is larger than that at the trough, and positive at the crest while negative at the trough, significant net growth over one long wavelength may be achieved. In addition to the conventional sideband instability, multiple resonant bands of instability are found both analytically and numerically for the modulated nonlinear Schrödinger equation.

The linear resonance condition (see (3.13) and (3.14)) with respect to the $2N\pi$ instability reveals that it is a new type of instability which belongs neither to Class I nor Class II (see McLean *et al.* 1981; Yuen & Lake 1982). The first multiple resonant band ($N = 1$) results from a quintet resonant interaction, among four short waves and one long wave. The second band ($N = 2$) is due to a sextet resonance, and so on. For weakly nonlinear waves the intensity of the resonances decreases as N increases. We find that for smaller values of the long- and short-wave slopes, and relatively large values of the wavelength ratio, the 2π instability (quintet resonance) is weaker than the Benjamin–Feir instability (quartet resonance). As the wave slope increases and/or wavelength ratio decreases, its strength increases to become comparable to that of the latter.

Similar to the relationship between the conventional sideband instability and the well-known quartet resonance (Phillips 1960; Hasselmann 1962), the $2N\pi$ instability is related to a new type of resonance for energy transfer among ocean waves. For short waves riding on a steep long wave, the energy transfer rate due to this new quintet resonance ($N = 1$) can be comparable to that of the well-known quartet resonance. Hence, this new resonance may be particularly important for the energy

transfer among waves with wavelengths much shorter than the peak wavelength of the spectrum.

While the nonlinear Schrödinger equation has been shown to be a useful asymptotic evolution equation for weakly nonlinear waves, its limitations are also well known and should be mentioned here. It is restricted to describing narrowbanded weakly nonlinear waves. Numerical solutions have shown that initial conditions satisfying these constraints may evolve to produce strongly nonlinear waves outside the region of validity of the equation. There is some evidence of similar difficulties in the problem treated here, with the perturbation wavenumbers of the multiple resonant bands being rather large for the small values of the perturbation parameters at which we expect the modulated nonlinear Schrödinger equation to be most accurate. The limitations of the nonlinear Schrödinger equation have, in the past, been addressed by going to higher-order formulations using Dysthe's (1979) equation or Zakharov's (1968) equation or their variants. Numerical solutions of Zakharov's equation (Yuen & Lake 1982) show that good quantitative agreement with the stability diagram based on the nonlinear Schrödinger equation is achieved for wave slopes of $O(10^{-2})$, but significant quantitative differences occur for wave slopes as small as 0.1. Thus we expect that while the formulation and results given here describe the essential physics, quantitative results, especially at the larger values of the perturbation parameters, must await independent confirmation.

During the writing of this paper we learned of similar work by our colleagues M. Naciri & C. C. Mei (personal communication) who are studying the interaction between short waves and long Gerstner waves using a Lagrangian formulation. Their results on the stability of the short-wave envelope appear to be similar to those presented here, but they have extended the work to consider the evolution of the short-wave envelope.

2. Formulation

2.1. *Modulated nonlinear Schrödinger equation*

A two-dimensional weakly nonlinear short-gravity-wave train is riding on and propagating in the same direction as a two-dimensional finite-amplitude periodic long wave in deep water. It is assumed that the flow is incompressible and irrotational and that the pressure is constant at the surface. The rectilinear coordinates (x, z) move with the long wave at its phase velocity with $z = 0$ fixed at the calm water level. The orthogonal curvilinear coordinates (s, n) are related to the (x, z) coordinates by a conformal mapping so that horizontal and vertical lines in the (s, n)-plane project onto the streamlines and equipotentials of the long wave (in the absence of the short wave) in the (x, z) plane, with $n = 0$ corresponding to the long-wave surface. The scale factor for the orthogonal coordinates $H(s, n)$ is defined by

$$H(s, n) = \Delta n/\Delta n_d = \Delta s/\Delta s_d, \tag{2.1}$$

where Δs, Δn, Δs_d and Δn_d are increments in s and n in the (s, n)-plane, and their projections on the (x, y)-plane, respectively. ϵ_1 and ϵ_2 are defined as the steepness of the long wave, and the steepness of the short-wave train at the trough of the long wave, respectively. ϵ_3 is the ratio of the short wavelength (at the trough of the long wave) to the long wavelength. The relationship between these parameters is assumed to be

$$\epsilon_1 = O(\epsilon_2^{\frac{1}{2}}), \quad \epsilon_3 = O(\epsilon_2^{\frac{3}{2}}). \tag{2.2}$$

The modulated nonlinear Schrödinger equation, describing the evolution of a short-wave train riding on a long wave, was derived by ZM:

$$\frac{\mathrm{d}b}{\mathrm{d}t}+\frac{H_0^2 g_1 b R_c}{2\sigma k_0}\frac{\partial}{\partial s}\left(\frac{\sigma}{g_1}\right)=-\mathrm{i}\left\{\frac{g_1}{2\sigma}\left[\frac{\partial}{\partial t}+\frac{H_0^2 R_c}{k_0}\frac{\partial}{\partial s}\right]\left[\frac{1}{g_1}\left(\frac{\partial}{\partial t}+\frac{H_0^2 R_c}{k_0}\frac{\partial}{\partial s}\right)b\right]+\tfrac{1}{2}\epsilon_2^2 b^2 b^* D\frac{H_0^4 k^4}{\sigma}\right\}, \tag{2.3}$$

where

$$\frac{\mathrm{d}}{\mathrm{d}t}=\frac{\partial}{\partial t}+\left(H_0^2 R_c+\frac{\sigma}{2k}\right)\frac{1}{k_0}\frac{\partial}{\partial s} \tag{2.4}$$

is the total derivative with respect to time, describing the rate of change for an observer moving at the group velocity of the short-wave train in the moving coordinates;

$$D=1+\frac{4H_0 R_c}{\sigma k_0}\frac{\partial H}{\partial n}\bigg|_{n=0}\sim 1+O(\epsilon_1\epsilon_3^{\frac{1}{2}}), \tag{2.5}$$

$$H_0=H(s,0), \tag{2.6}$$

and R_c is the phase velocity ratio of the long wave to the short wave (at the trough of the long wave); b, σ, k and g_1, represent the potential amplitude, intrinsic frequency and wavenumber of the short-wave train, and the effective gravitational acceleration†, respectively. The variables along the long-wave surface are normalized by their respective values at the trough of the long wave, which are denoted by an additional subscript '0'. For example, σ_0 is the intrinsic frequency of the short-wave train at the trough of the long wave before the normalization, and σ is the normalized value. The time t is non-dimensionalized by σ_0. The long wavelength is normalized so that the long wavenumber $K_d=1$ and consequently the short wavenumber (at the trough of the long wave) $k_0=(\epsilon_3^{-1}H_{00}^{-1})\sim O(\epsilon_3^{-1})$.

If the long wave is weakly nonlinear and the wavelength ratio is very small (as defined in (4.1)), equation (2.3) reduces to the same form as the conventional Schrödinger equation but with coefficients which vary periodically along the long wave:

$$\frac{\partial a^{(11)}}{\partial t}+Q_1\frac{\partial a^{(11)}}{\partial s}=-\mathrm{i}\left\{Q_2\frac{\partial^2 a^{(11)}}{\partial s^2}+Q_3 a^{(11)^2}a^{(11)^*}\right\}, \tag{2.7}$$

where $a^{(11)}$ is the leading-order first harmonic amplitude of the short wavetrain,

$$a^{(11)}=b\sigma/g_1, \tag{2.8a}$$

and

$$Q_1=\sigma\frac{(R_c+\frac{1}{2})}{kk_0}=\frac{-\epsilon_3^{\frac{1}{3}}(1+\frac{3}{2}\epsilon_1-\frac{9}{8}\epsilon_1^2-\frac{1}{2}\epsilon_3^{\frac{1}{3}}-\frac{1}{2}\epsilon_3^{\frac{1}{3}}\epsilon_1)}{1+2\epsilon_1(1+\cos s)+4\epsilon_1^2(\cos s+\cos 2s)}, \tag{2.8b}$$

$$Q_2=\frac{\sigma}{8k^2k_0^2}=\frac{\epsilon_3^2(1+2\epsilon_1-\epsilon_1^2)}{8[1+2\epsilon_1(1+\cos s)+4\epsilon_1^2(\cos s+\cos 2s)]^2}, \tag{2.8c}$$

$$Q_3=\tfrac{1}{2}\epsilon_2^2[1+2\epsilon_1(1+\cos s)+4\epsilon_1^2(\cos s+\cos 2s)]^2. \tag{2.8d}$$

The steady solution of the short wavetrain can be obtained from (2.3). For detailed information about the derivation of (2.3) and its steady solution, see ZM and Zhang (1990).

† Note that our effective gravitational acceleration defined in (A 1) is different from that of Longuet-Higgins (1987) by a factor H_0^{-1} due to the coordinates (s,n).

2.2. *Governing equation for sideband instability*

We consider a pair of sideband disturbances superposed on the steady solution of a short wavetrain and then investigate their resonant growth. We take the solution of (2.3) to be

$$\tilde{b} = b(1+B) = |b|\,e^{i\tilde{\theta}}(1+B), \tag{2.9}$$

where $|b|\,e^{i\tilde{\theta}}$ is the steady solution and B represents the superposed disturbances of infinitesimal initial amplitude.

Substituting (2.9) into (2.3), and subtracting the steady solution we obtain the equation governing the evolution of the disturbances:

$$\begin{aligned}\frac{dB}{dt} = -i\Big\{&\frac{1}{\sigma b}\Big[\frac{db}{dt}\frac{dB}{dt} - \frac{\sigma}{2kk_0}\Big(\frac{\partial b}{\partial s}\frac{dB}{dt} + \frac{db}{dt}\frac{\partial B}{\partial s}\Big) + \frac{\sigma^2}{4k^2k_0^2}\frac{\partial B}{\partial s}\frac{\partial b}{\partial s}\Big] \\ &- \frac{H_0^2 R_c}{2\sigma g_1 k_0}\frac{\partial g_1}{\partial s}\frac{dB}{dt} + \frac{H_0^2 R_c}{8kg_1 k_0^2}\frac{\partial g_1}{\partial s}\frac{\partial B}{\partial s} + \frac{1}{2\sigma}\frac{d^2B}{dt^2} - \frac{1}{2kk_0}\frac{\partial}{\partial s}\Big(\frac{dB}{dt}\Big) \\ &+ \frac{\sigma}{8kk_0^2}\frac{\partial}{\partial s}\Big(\frac{1}{k}\frac{\partial B}{\partial s}\Big) + \frac{\epsilon_2^2|b|^2H_0^4k^4}{2\sigma}D(B+B^*) + O(\epsilon_2^2)|B|^2\Big\}.\end{aligned} \tag{2.10}$$

The right-hand side of (2.10) describes the rate of change of the disturbances with respect to time. Neglecting terms of $O(\epsilon_2^3)B$, (2.10) reduces to

$$\frac{dB}{dt} = -i\Big[\frac{\sigma}{8kk_0^2}\frac{\partial}{\partial s}\Big(\frac{1}{k}\frac{\partial B}{\partial s}\Big) + \frac{\epsilon_2^2|b|^2H_0^4k^4}{2\sigma}D(B+B^*)\Big]. \tag{2.11}$$

The derivation of (2.11) is given in detail by Zhang (1990). Equation (2.11) will be used to study the resonant growth of sideband disturbances superposed on the short-wave train.

3. Resonant growth of disturbances

3.1. *Local resonant growth rate and relative phase*

In anticipation of a changing relative phase between the upper- and lower-band disturbances, and following Benjamin & Feir (1967), we let

$$B = |p_1|\,e^{i(\beta-\gamma_1)} + |p_2|\,e^{-i(\beta+\gamma_2)}, \tag{3.1}$$

where $|p_1|$ and $|p_2|$ are the amplitudes of the upper and lower sidebands, respectively, and may grow with time; $\beta-\gamma_1$ and $\beta+\gamma_2$ are phase angles, $d\beta/dt = 0$ and $(1/k_0)(\partial\beta/\partial s) = \tilde{K}$ is the perturbation wavenumber; $(\gamma_1+\gamma_2)$ represent the relative phase and may vary along the long wave.

Substituting (3.1) into (2.11) and neglecting terms of $O(\epsilon_2^3|p|)$, we obtain two equations with respect to $e^{i\beta}$ and $e^{-i\beta}$. Splitting these equations into real and imaginary parts and adding the imaginary parts, we obtain coupled equations describing the resonant growth rate and the variation of the relative phase angle $(\gamma_1+\gamma_2)$:

$$\frac{d|p_1|}{dt} = \tfrac{1}{2}\epsilon_2^2 D\frac{|b|^2k^4H_0^4}{\sigma}\sin(\gamma_1+\gamma_2)\,|p_2|, \tag{3.2a}$$

$$\frac{d|p_2|}{dt} = \tfrac{1}{2}\epsilon_2^2 D\frac{|b|^2k^4H_0^4}{\sigma}\sin(\gamma_1+\gamma_2)\,|p_1|, \tag{3.2b}$$

$$\frac{d(\gamma_1+\gamma_2)}{dt} = \epsilon_2^2 D\frac{|b|^2k^4H_0^4}{\sigma} - \frac{\sigma\tilde{K}^2}{4k^2} + \frac{(|p_1|^2+|p_2|^2)}{2|p_1|\,|p_2|}\frac{\epsilon_2^2 D\,|b|^2k^4H_0^4}{\sigma}\cos(\gamma_1+\gamma_2). \tag{3.3}$$

For simplicity we assume that the amplitudes of the upper and lower sideband are the same initially. Then (3.2a, b) and (3.3) may be simplified to

$$\frac{1}{|p|}\frac{\mathrm{d}|p|}{\mathrm{d}t} = \tfrac{1}{2}\epsilon_2^2 D\frac{|b|^2k^4H_0^4}{\sigma}\sin(\gamma_1+\gamma_2), \tag{3.4}$$

$$\frac{\mathrm{d}(\gamma_1+\gamma_2)}{\mathrm{d}t} = \epsilon_2^2 D\frac{|b|^2k^4H_0^4}{\sigma}[1+\cos((\gamma_1+\gamma_2)] - \frac{\sigma\tilde{K}^2}{4k^2}. \tag{3.5}$$

Given the perturbation wavenumber $\tilde{K}$ and the scale parameters ϵ_1, ϵ_2, ϵ_3, we may solve (3.5) for $(\gamma_1+\gamma_2)$ by numerical iteration. Because of the coupling between $|p_1|$ and $|p_2|$ as shown in (3.2a) and (3.2b), $|p_1|$ and $|p_2|$ will eventually equilibrate even if initially $|p_1| \neq |p_2|$. Cross-multiplying (3.2a) and (3.2b) by $|p_1|$ and $|p_2|$, respectively, gives $\mathrm{d}/\mathrm{d}t(|p_1|^2-|p_2|^2) = 0$. Hence if $(|p_1|+|p_2|)$ grows exponentially with time, the magnitude of $(|p_1|-|p_2|)$ decreases exponentially and the disturbance amplitudes equilibrate. Hence our assumption that $|p_1| = |p_2|$ does not lack generality.

3.2. *Floquet system and multiple resonant bands*

The coefficients in the coupled ordinary differential equations (3.4) and (3.5) are periodic in time and in space. Equations (3.4) and (3.5) thus form a Floquet system (Drazin & Reid 1981). It is well known that a Floquet system may have multiple resonant regions (Magnus & Winkler 1966; Iooss & Joseph 1980). We found that a short-wave train riding on a long wave is unstable to multiple bands of perturbation wavenumbers, in contrast to only a single sideband in the case of an equivalent wave train travelling on otherwise calm water. (The sidebands near the higher harmonics of the wave train are not to be confused with the multiple resonant bands described here.) We elucidate below the causes of these multiple resonant bands.

The resonant band (in the neighbourhood of $\tilde{K} = 0$) corresponds to the conventional sideband instability, and the relative phase $(\gamma_1+\gamma_2)$ fluctuates slightly around a constant value and is periodic with respect to the long wave. For perturbation wavenumbers displaying a significant growth rate, solutions of (3.5) show that $(\gamma_1+\gamma_2)$ converges very quickly and depends only on the position at the long-wave surface, regardless of its initial value. The rapid convergence indicates that the phase angle is possibly a steady function of the position on the long wave, which is confirmed in the stability analysis of the relative phase presented in §3.4. As a result, the growth rate of the disturbances computed from (3.4) is also periodic and steady with respect to the long wave.

With a further increase of $\tilde{K}$, $(\gamma_1+\gamma_2)$ continuously decreases along the long wave and hence can no longer be periodic with respect to the long wave. Within certain ranges of $\tilde{K}$, the decrease of $(\gamma_1+\gamma_2)$ may be $2N\pi$ (N a positive integer) after the disturbance travels one long wavelength. Hence, the sine and cosine functions of $(\gamma_1+\gamma_2)$ appearing in (3.4) and (3.5) are periodic and steady with respect to the long wave. Consequently, the local resonant growth rate is also periodic and steady. The local resonant growth rate given by (3.4) will change sign $2N$ times in one long wavelength. Without the modulation by the long wave, the resonant growth rate simply varies sinusoidally, and hence the net resonant growth of the disturbances is zero. With the modulation by the long wave, however, the magnitude of the local resonant growth rate becomes larger at the crest and smaller at the trough of the long wave. If, for $N = 1$, the phase changes along the long-wave surface so that the local growth rate is positive near the crest and negative near the trough of the long wave, then the net resonant growth of the disturbances may still be significant. Thus a

short-wave train riding on a periodic long wave may have multiple regions of instability.

We also expect that more general instabilities may exist. That is, the relative phase may decrease $2N'\pi$ after the disturbances travel M long wavelengths, where M and N' are integers. The aforementioned $2N\pi$ instabilities can be viewed as a special case when $N'/M = N$. When N'/M is not an integer, the instabilities are found to be insignificant.

3.3. *Global resonant growth – Floquet exponent*

We have shown that the resonant growth rate of a pair of disturbances may change along the long-wave surface, in magnitude alone for the conventional sideband instability, but in both magnitude and sign for the $2N\pi$ instabilities. Thus a pair of disturbances with the maximum resonant growth rate along part of the long-wave surface do not necessarily grow fastest nor even have a net growth along the entire long-wave surface. To measure their overall resonant growth along the long wave, we use the global resonant growth, G, which is defined as the logarithmic resonant growth after the disturbances travel one long wavelength (in the moving coordinates). This index is known as the Floquet exponent for studying the stability of solutions which depend periodically on time (Iooss & Joseph 1980).

Since the resonant growth rate is steady relative to the long-wave surface and the disturbances travel at the group velocity of the short-wave train, then global resonant growth is given by

$$G = \frac{1}{2\pi}\ln\left|\frac{p(2\pi)}{p(0)}\right| = \frac{1}{2\pi}\int_0^{2\pi} \frac{\frac{1}{|p|}\frac{\mathrm{d}|p|}{\mathrm{d}t}k_0}{\left(R_c H_0^2 + \frac{\sigma}{2k}\right)}\mathrm{d}s. \tag{3.6}$$

3.4. *Steady relative phase and global resonant growth*

To show that the relative phase of disturbances displaying a global resonant growth must be steady relative to the long-wave surface, we assume that the solution for (3.5), $\bar{\gamma}$, is disturbed by a time-dependent perturbation $\tilde{\gamma}$:

$$(\gamma_1+\gamma_2) = \bar{\gamma}+\tilde{\gamma}. \tag{3.7}$$

Substituting (3.7) into (3.5), we obtain

$$\frac{\mathrm{d}\tilde{\gamma}}{\mathrm{d}t} = \epsilon_2^2 D\frac{|b|^2k^4H_0^4}{\sigma}[\cos\bar{\gamma}(\cos\tilde{\gamma}-1)-\sin\bar{\gamma}\sin\tilde{\gamma}]. \tag{3.8}$$

If $\tilde{\gamma} \ll 1$, (3.8) may be approximated by

$$\frac{\mathrm{d}\tilde{\gamma}}{\mathrm{d}t} = -\left[\epsilon_2^2 D\frac{|b|^2k^4H_0^4}{\sigma}\sin\bar{\gamma}\right]\tilde{\gamma}. \tag{3.9}$$

Making use of (3.4) and (3.6), an approximate solution for $\tilde{\gamma}$ is

$$\tilde{\gamma}(2\pi) = \tilde{\gamma}(0)\,\mathrm{e}^{-4\pi G}. \tag{3.10}$$

For globally growing disturbances, $G > 0$ and hence $|\tilde{\gamma}(2\pi)| < |\tilde{\gamma}(0)|$. That is, the phase perturbation decreases after disturbances travel one long wavelength, and hence the solution of $(\gamma_1+\gamma_2)$ is steady. Conversely, if the solution of $(\gamma_1+\gamma_2)$ is steady, then $G > 0$ according to (3.10), indicating the disturbances experience resonant growth after travelling one long wavelength. To search for resonant regions, therefore, we only need to search for disturbances whose relative phases are steady relative to the long wave.

3.5. *Linear resonance condition*

By recalling the phase function of the disturbance defined in (2.9) and (3.1), the sums of the wavenumbers and absolute frequencies of the upper- and lower-sideband disturbances are given by

$$k_u + k_\ell = 2k - \frac{\partial(\gamma_1+\gamma_2)}{\partial s}, \tag{3.11}$$

$$\omega_u + \omega_\ell = 2\omega + \frac{\partial(\gamma_1+\gamma_2)}{\partial t} \tag{3.12}$$

where ω is the absolute frequency defined in (4.6), and the subscripts u and ℓ represent the upper- and lower-sideband disturbances.

The linear resonance condition of the $2N\pi$ instability is derived by averaging (3.11) and (3.12) over one long wavelength. Since $(\gamma_1+\gamma_2)$ decreases by $2N\pi$ while the disturbances travel one long wavelength, (3.11) reduces to

$$k_u + k_\ell + NK_d = 2k. \tag{3.13}$$

Noticing the relationship between the absolute frequency and the intrinsic frequency (see (4.6)) and with the relative phase between the resonant upper- and lower-sideband disturbances being steady, with the help of (3.13), equation (3.12) reduces to

$$\sigma_u + \sigma_\ell + N\Omega_d = 2\sigma, \tag{3.14}$$

where Ω_d is the long-wave frequency in the fixed coordinates. Equations (3.13) and (3.14) describe the linear resonance condition for the $2N\pi$ instability. For $N = 0$, the linear resonance condition displays a quartet resonance, or more generally, the class I ($m = 1$) instability. For $N = 1, 2, \ldots,$ it indicates a quintet, sextet, ... resonance. These resonances are different from class I and II instabilities defined by McLean *et al.* (1981). For example, the 2π instability involves five waves, but it is clearly different from the Class II ($m = 1$) instability.

It is well known that resonances involving more waves are usually weaker if the steepness of the primary wave is not large (McLean *et al.* 1981; Yuen & Lake 1982). This trend is also observed in our analytical and numerical results. That is, the 2π instability is weaker than the conventional sideband instability, and the 4π instability is weaker than the 2π instability, unless the short- and long-wave steepnesses are large.

Using the same approach, we also derive the linear resonance condition for the $2(N/M)\pi$ instability:

$$M(k_u + k_\ell) + NK_d = 2Mk, \tag{3.15}$$

$$M(\sigma_u + \sigma_\ell) + N\Omega_d = 2M\sigma. \tag{3.16}$$

For a non-integer N/M, the lowest number of wave modes involved in the $2(N/M)\pi$ instability is nine ($M = 2$, $N = 1$). Hence, this type of instability is expected to be very weak, consistent with the results in §§4 and 5.

4. Approximate analytical solutions

In order to examine and confirm the numerical stability computations, we also derive the corresponding analytical solutions. For simplicity, we consider the sideband instability of a weakly nonlinear short-wave train riding on a much longer

weakly nonlinear wave. Accordingly, in this section, the range of the scale parameters defined in (2.2) is restricted to

$$\epsilon_1 = O(\epsilon_2), \quad \epsilon_3 = O(\epsilon_2^3). \tag{4.1}$$

When the long-wave steepness is small, an approximate analytical solution for the long-wave velocity field and elevation is used to solve the modulated nonlinear Schrödinger equation for the variation of a steady short-wave train along the long wave. The relative variation of the short-wave intrinsic frequency along the long wave is found to be $O(\epsilon_1^3)$, much smaller than $O(\epsilon_1^2)$ as previously shown by Phillips (1981). Hence, we may approximate the short-wave intrinsic frequency as a constant along the long-wave surface, resulting in a great simplification in the analytical solution. We then use (3.4) and (3.5) to obtain the analytical solution for the conventional sideband, $2N\pi$ and $2(N/M)\pi$, instabilities.

4.1. *Approximate solution for undisturbed long wave*

In the coordinates moving with its phase velocity C, the long wave is steady. The function mapping the (s,n)-coordinates to the (x,y)-coordinates is given approximately by

$$\left.\begin{aligned} x &= s+\epsilon_1 \mathrm{e}^n \sin s+\epsilon_1^2 \mathrm{e}^{2n} \sin 2s+O(\epsilon_1^3), \\ z &= n-\tfrac{1}{2}\epsilon_1^2+\epsilon_1 \mathrm{e}^n \cos s+\epsilon_1^2 \mathrm{e}^{2n} \cos 2s+O(\epsilon_1^3). \end{aligned}\right\} \tag{4.2}$$

where s and n are related to the potential Φ and stream function Ψ of the long wave through $s = -\Phi/|C|$, $n = -\Psi/|C|$. The scale factor of the orthogonal curvilinear coordinates is equal to the ratio of the particle velocity $U(s,n)$ of the long wave to its phase velocity C (Zhang 1990):

$$H(s,n) = U(s,n)/C = [1+2\epsilon_1 \mathrm{e}^n \cos s+\epsilon_1^2 \mathrm{e}^{2n}+4\epsilon_1^2 \mathrm{e}^{2n} \cos 2s]^{-\frac{1}{2}}. \tag{4.3}$$

Thus the normalized $H_0(s)$ is given by

$$H_0 = [1+2\epsilon_1(1+\cos s)+4\epsilon_1^2(\cos s+\cos 2s)]^{-\frac{1}{2}}. \tag{4.4}$$

4.2. *Steady solution for modulated short wave*

The linear dispersion relation between the intrinsic frequency and the wavenumber is given by

$$\sigma^2 = H_0^2 g_1 k. \tag{4.5}$$

The absolute frequency of the short wave riding on the long-wave surface is equal to the sum of the intrinsic frequency and the Doppler frequency shift due to the advection by the long-wave particle velocity:

$$\omega = \sigma + H_0^2 Ck. \tag{4.6}$$

The fractional derivatives of g_1 and σ along the long-wave surface are

$$\frac{1}{g_1}\frac{\partial g_1}{\partial s} \approx O(\epsilon_1^3), \tag{4.7}$$

and

$$\frac{1}{\sigma}\frac{\partial \sigma}{\partial s} \approx \frac{1}{2g_1}\frac{\partial g_1}{\partial s} \sim O(\epsilon_1^3). \tag{4.8}$$

The derivation of (4.7) and (4.8) is given in Appendix A. We may approximate both g_1 and σ by unity along the long wave to the same order of accuracy as the mapping function. The small variation of g_1 is due to its definition in the orthogonal

curvilinear coordinates (A 1), whereas the small modulation of the short-wave intrinsic frequency is independent of the coordinates. However, this result may not be valid when the water depth is not large compared with the long wavelength.

According to the linear dispersion relationship (4.5), the normalized wavenumber is given by

$$k = H_0^{-2} = 1 + 2\epsilon_1(1+\cos s) + 4\epsilon_1^2(\cos s + \cos 2s) + O(\epsilon_1^3). \tag{4.9}$$

Splitting the nonlinear Schrödinger equation (2.3) into real and imaginary parts, which represent the wave-action conservation and nonlinear dispersion relationship, respectively, and solving these two simultaneous equations, we find that the normalized (potential) amplitude $|b|$ is given by

$$|b| = 1 + O(\epsilon_1^3, \epsilon_1\epsilon_2^2). \tag{4.10}$$

According to (2.8a), the short-wave steepness is given by

$$|a^{(11)}|\, k = 1 + 2\epsilon_1(1+\cos s) + 4\epsilon_1^2(\cos s + \cos 2s) + O(\epsilon_1^3, \epsilon_2^2\epsilon_1). \tag{4.11}$$

These approximate solutions are consistent with the numerical results of ZM.

4.3. *Instabilities*

Making use of (2.8a), (4.5) and (4.8) and neglecting the higher-order terms, we simplify (3.4) and (3.5) to

$$\frac{1}{|p|}\frac{\mathrm{d}|p|}{\mathrm{d}t} = \tfrac{1}{2}\epsilon_2^2 a^{(11)^2}k^2 \sin(\gamma_1+\gamma_2) + O(\epsilon_2^5), \tag{4.12}$$

$$\frac{\mathrm{d}(\gamma_1+\gamma_2)}{\mathrm{d}t} = \epsilon_2^2 a^{(11)^2}k^2[1+\cos(\gamma_1+\gamma_2)] - \frac{\tilde{K}^2}{4k^2} + O(\epsilon_2^5). \tag{4.13}$$

In solving (4.13), the following equations and approximations are used.

(a) For a pair of resonant disturbances the relative phase $(\gamma_1+\gamma_2)$ is represented by

$$(\gamma_1+\gamma_2) = \gamma_0 + (N/M)\,s + \sum_{n=1}^{\infty}[c_n \sin(n/M)\,s + d_n \cos(n/M)\,s], \tag{4.14}$$

where γ_0 is a constant; n, N and M are integers; c_n and d_n are Fourier coefficients and assumed to be small. When $N = 0$, the relative phase fluctuates around γ_0 and is periodic with respect to the long wave, corresponding to the conventional sideband instability. With $N \neq 0$ and $M = 1$, the decrease in the phase is $2N\pi$ after the disturbances travel one long wavelength, corresponding to the $2N\pi$ instability. When $N \neq 0, M \neq 1$ and N/M is a non-integer number, the decrease in the phase is $2N\pi$ after the disturbances travel M long wavelengths, corresponding to a $2(N/M)\pi$ instability.

(b) It is shown in §3.4 that the relative phase, $(\gamma_1+\gamma_2)$, of a pair of resonant disturbances is steady relative to the long wave. Thus,

$$\frac{\mathrm{d}(\gamma_1+\gamma_2)}{\mathrm{d}t} = \left(H_0^2 R_c + \frac{\sigma}{2k}\right)\frac{1}{k_0}\frac{\partial(\gamma_1+\gamma_2)}{\partial s}. \tag{4.15}$$

(c) Based on phase conservation, the ratio of the perturbation wavenumber to the short wavenumber may be approximated by

$$\tilde{K}/2k = \epsilon_2 q\,(1 + O(\epsilon_1^3\epsilon_3^{\frac{1}{3}})), \tag{4.16}$$

where q is a constant along the long-wave surface.

We first solve (4.13) for $(\gamma_1+\gamma_2)$, and then obtain the resonant growth rate along the long wave through (4.12). Finally, the global resonant growth is computed through (3.6). To show the influence of the modulation on the stability of the short-wave train, we compare the instabilities of the short-wave train riding on the long wave with the Benjamin–Feir instability of an equivalent wave train advancing on otherwise calm water. Following Longuet-Higgins (1987), the equivalent wave train is defined to have the same wavelength and steepness as the short-wave train at the intersection of the long-wave surface and the calm water level. Therefore, the analytical solutions of the resonant growth rate, global resonant growth and perturbation wavenumber of the disturbances (to a short-wave train riding on a long wave) are expressed in terms of ratios to those of the equivalent wave. The details of ratios are described in Appendix B.

4.3.1. *Conventional sideband instability*

(*a*) The relative phase along the long wave:

$$(\gamma_1+\gamma_2) = \gamma_0 - 4\epsilon_1\epsilon_2^2 T^{-1}(1+2\epsilon_1)q^2\sin s + 4\epsilon_1\epsilon_2^4 T^{-2}(1+8\epsilon_1)q^2\sin\gamma_0\cos s - 7\epsilon_1^2\epsilon_2^2 T^{-1}q^2\sin 2s + 9.5\epsilon_1^2\epsilon_2^4 T^{-2}q^2\sin\gamma_0\cos 2s + O(\epsilon_1^3, \epsilon_1\epsilon_2^6 T^{-3}), \quad (4.17)$$

where

$$\gamma_0 = \arccos\left[\frac{q^2(1+2\epsilon_1)-1-6\epsilon_1-18\epsilon_1^2+12\epsilon_1^2\epsilon_2^4 T^{-2}q^2\sin^2\gamma_0}{1+6\epsilon_1+18\epsilon_1^2-4\epsilon_1^2\epsilon_2^4 T^{-2}q^4}\right] \quad (4.18)$$

and

$$T = \left|\frac{R_c+\frac{1}{2}}{k_0}\right| \sim O(\epsilon_3^{\frac{1}{3}}). \quad (4.19)$$

(*b*) The global resonant growth:

$$G = (1+8\epsilon_1^2-4\epsilon_1^2\epsilon_2^4 T^{-2}q^4)\sin\gamma_0 + 6\epsilon_1^2\epsilon_2^4 T^{-2}q^2\sin 2\gamma_0. \quad (4.20)$$

(*c*) The bandwidth of resonant perturbation wavenumber:

$$|q_b| \leqslant \sqrt{2}(1+4\epsilon_1^2-4\epsilon_1^2\epsilon_2^4 T^{-2}). \quad (4.21)$$

(*d*) The perturbation wavenumber for the maximum global growth:

$$q_{\max} = 1+4\epsilon_1^2-6\epsilon_1^2\epsilon_2^4 T^{-2}. \quad (4.22)$$

(*e*) For $q = q_{\max}$, the maximum global growth $G_{\max}$ is given by

$$G_{\max} = 1+8\epsilon_1^2-4\epsilon_1^2\epsilon_2^4 T^{-2}, \quad (4.23)$$

and the corresponding resonant growth rate along the long wave is given by

$$\frac{1}{|p|}\frac{\mathrm{d}|p|}{\mathrm{d}t}\bigg|_{q=q_{\max}} = 1+4\epsilon_1^2-4\epsilon_1^2\epsilon_2^4 T^{-2}+4\epsilon_1\cos s+(10\epsilon_1^2+4\epsilon_1^2\epsilon_2^4 T^{-2})\cos 2s. \quad (4.24)$$

4.3.2. $2N\pi$ *instability*

The strongest $2N\pi$ instability occurs when $N = 1$. For simplicity, we only give the solution for $N = 1$ in detail.

(*a*) The relative phase along the long wave:

$$\begin{aligned}(\gamma_1+\gamma_2) = \gamma_0 + s + [2\epsilon_1 - \epsilon_2^2 T^{-1}(1+6\epsilon_1)\cos\gamma_0 - 4\epsilon_1\epsilon_2^2 T^{-1}]\sin s \\ - \epsilon_2^2 T^{-1}(1+6\epsilon_1)\sin\gamma_0\cos s + [2\epsilon_2^2 - 2\epsilon_1\epsilon_2^2 T^{-1}\cos\gamma_0 \\ + 0.25\epsilon_2^4 T^{-2}\cos 2\gamma_0]\sin 2s - [2\epsilon_1\epsilon_2^2 T^{-1}\sin\gamma_0 \\ - 0.25\epsilon_2^4 T^{-2}\sin 2\gamma_0]\cos 2s + O(\epsilon_1^3, \epsilon_2^6 T^{-3}), \end{aligned} \quad (4.25)$$

where

$$\gamma_0 = \arccos\left[\frac{q^2(1+2\epsilon_1)-\epsilon_2^{-2}T-1-6\epsilon_1-18\epsilon_1^2-0.5\epsilon_2^2T^{-1}(1+12\epsilon_1)}{2\epsilon_1(1+6\epsilon_1+\epsilon_2^2T^{-1})}\right]. \quad (4.26)$$

(*b*) The global growth:

$$G = 2\epsilon_1(1+\epsilon_2^2T^{-1})\sin\gamma_0 + O(\epsilon_1^3, \epsilon_2^6T^{-3}). \quad (4.27)$$

(*c*) The bandwidth of resonant perturbation wavenumber:

$$[q_{\max}^2 - 2\epsilon_1(1+\epsilon_2^2T^{-1})]^{\frac{1}{2}} \leqslant q_b \leqslant [q_{\max}^2 + 2\epsilon_1(1+\epsilon_2^2T^{-1})]^{\frac{1}{2}}, \quad (4.28)$$

where $q_{\max}$ is given by (4.29).

(*d*) The perturbation wavenumber related to the maximum global growth:

$$q_{\max} = \left[\frac{\epsilon_2^{-2}T}{1+6\epsilon_1+10\epsilon_1^2} + 1 + 8\epsilon_1^2 + 0.5\epsilon_2^2T^{-1}(1+6\epsilon_1)\right]^{\frac{1}{2}}. \quad (4.29)$$

(*e*) When $q = q_{\max}$, the maximum global growth G is given by

$$G_{\max} = 2\epsilon_1(1+\epsilon_2^2T^{-1}), \quad (4.30)$$

and the corresponding growth rate along the long wave is given by

$$\begin{aligned}\frac{1}{|p|}\frac{\mathrm{d}|p|}{\mathrm{d}t}\bigg|_{q=q_{\max}} &= \epsilon_1(1+2\epsilon_2^2T^{-1}) + (1+7.5\epsilon_1^2-0.25\epsilon_2^4T^{-2})\cos s \\ &\quad + 0.5\epsilon_1\epsilon_2^2T^{-1}\sin s + \epsilon_1(3-2\epsilon_2^2T^{-1})\cos 2s \\ &\quad + 0.5\epsilon_2^2T^{-1}(1+6\epsilon_1)\sin 2s + (8.5\epsilon_1^2-0.25\epsilon_2^4T^{-2})\cos 3s \\ &\quad + 2.5\epsilon_1\epsilon_2^2T^{-1}\sin 3s. \end{aligned} \quad (4.31)$$

For large $N(N \geqslant 2)$, only the order of magnitude of $G_{\max}$, $q_{\max}$, and q_b are given here:

$$G_{\max} = O(\epsilon_1^N), \quad (4.32)$$

$$q_{\max} = O(N\epsilon_2^{-2}T)^{\frac{1}{2}}, \quad (4.33)$$

$$[q_{\max}^2 - O(\epsilon_1^N)]^{\frac{1}{2}} \leqslant q_b \leqslant [q_{\max}^2 + O(\epsilon_1^N)]^{\frac{1}{2}}. \quad (4.34)$$

4.3.3. $2(N/M)\pi$ *Instability*

A comprehensive search for $2(N/M)\pi$ instabilities is laborious and has not been pursued. We have only considered the approximate solutions for the cases: (*a*) $N = 1$, $M = 2$, (*b*) $N = 1$, $M = 3$ and (*c*) $N = 2$, $M = 3$. Within the accuracy of our approximate solutions at order $O(\epsilon_1^2\epsilon_2^4T^{-2})$, no global resonant growth is found for all three cases, indicating that the $2(N/M)\pi$ instability of these cases is insignificant compared with $2N\pi$ instability.

5. Numerical solutions of the stability problem

5.1. *Comparison between analytical and numerical results*

It is of practical interest to study the characteristics of disturbances displaying a large global resonant growth along the long wave. Hence, the comparison is focused on those disturbances having a maximum global resonant growth (i.e. when

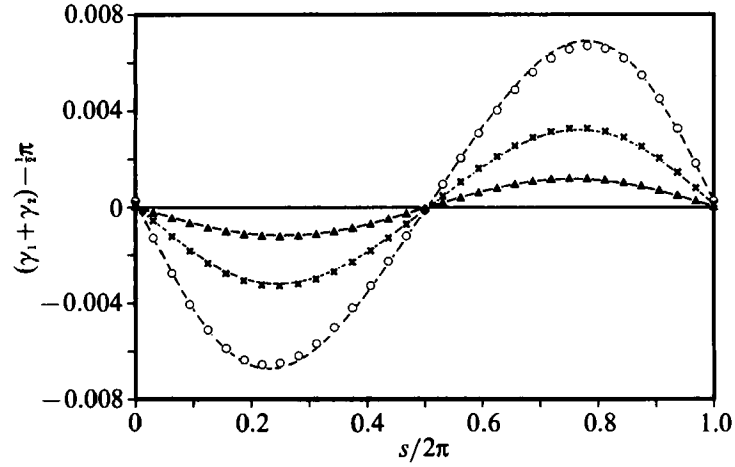

FIGURE 1. The relative phase $(\gamma_1+\gamma_2)_{SB}$ of sideband disturbances displaying a maximum global resonant growth is shown as a function of s for: $\epsilon_1 = 0.01$, $\epsilon_2 = 0.03$, and $\epsilon_3 = 0.001$ (——, analytical; △, numerical); $\epsilon_1 = 0.02$, $\epsilon_2 = 0.05$ and $\epsilon_3 = 0.005$ (— — —, analytical; ×, numerical); and $\epsilon_1 = 0.05$, $\epsilon_2 = 0.05$ and $\epsilon_3 = 0.01$ (– – –, analytical; ○, numerical).

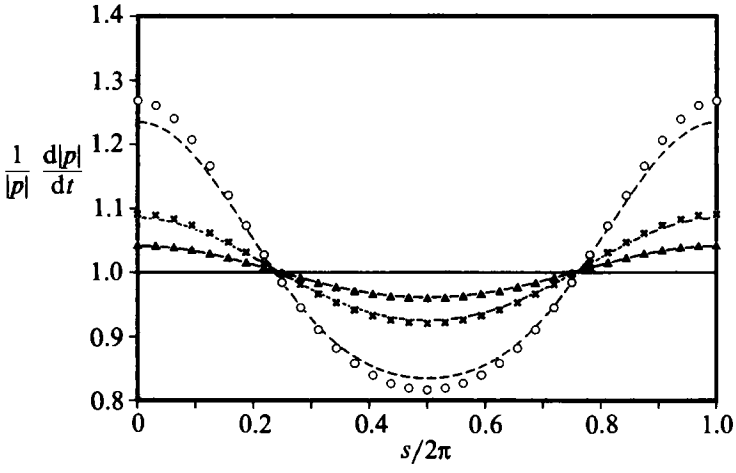

FIGURE 2. The resonant growth rate $(1/|p|)(d|p|/dt)|_{SB}$ is shown as a function s. Symbols are the same as figure 1.

$q = q_{max}$). The numerical results are also normalized by the corresponding results in the absence of the long wave. The details of the normalization are described in Appendix B.

For the conventional sideband instability the analytical solutions for the relative phase (4.17), and resonant growth rate (4.24), of disturbances when $q = q_{max}$ are compared with the related numerical results in figures 1 and 2, respectively. It is observed that the related analytical and numerical results are almost identical when the scale parameters ϵ_1, ϵ_2, and ϵ_3 are small. As these parameters increase, the discrepancy between numerical and analytical results gradually increases. Both the analytical solution (4.20) and the related numerical results of G as a function of q are shown in figure 3. The agreement between the analytical and numerical results is also satisfactory when ϵ_1, ϵ_2 and ϵ_3 are small.

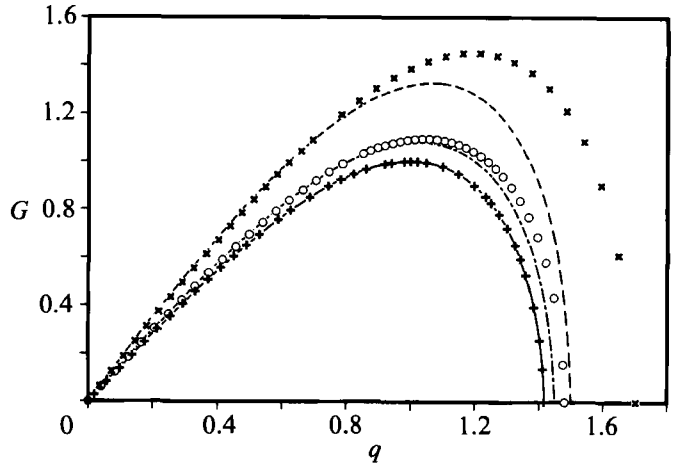

FIGURE 3. The global resonant growth of disturbance G_{SB} is shown as a function of the perturbation wavenumber q for: $\epsilon_1 = 0.01$, $\epsilon_2 = 0.03$, and $\epsilon_3 = 0.001$ (——, analytical; +, numerical); $\epsilon_1 = 0.1$, $\epsilon_2 = 0.1$ and $\epsilon_3 = 0.01$ (— — —, analytical; ○, numerical); and $\epsilon_1 = 0.2$, $\epsilon_2 = 0.1$ and $\epsilon_3 = 0.01$ (– –, analytical; ×, numerical).

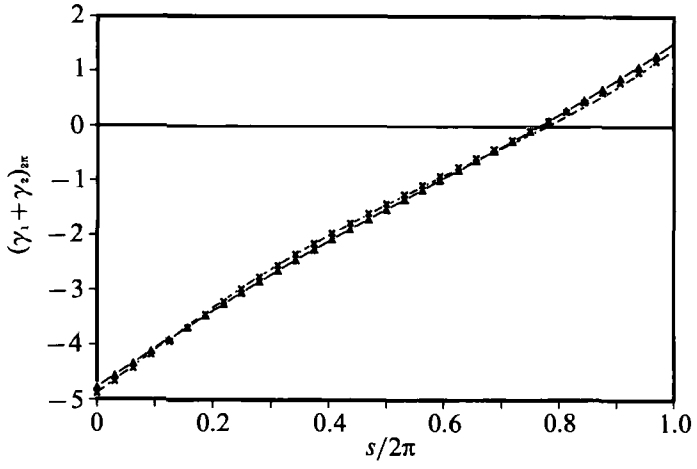

FIGURE 4. $(\gamma_1+\gamma_2)_{2\pi}$ of 2π disturbances displaying a maximum global resonant growth is shown as a function of s for: $\epsilon_1 = 0.05$, $\epsilon_2 = 0.03$ and $\epsilon_3 = 0.0005$ (——, analytical; △, numerical); and $\epsilon_1 = 0.10$, $\epsilon_2 = 0.10$ and $\epsilon_3 = 0.01$ (– – –, analytical; ×, numerical).

For the 2π instability, the approximate solutions for $(\gamma_1+\gamma_2)$ of (4.25), $(1/|p|)(\mathrm{d}|p|/\mathrm{d}t)$ of (4.31) when $q = q_{\max}$, and G of (4.27) are compared with the related numerical results in figures 4–6. When ϵ_1, ϵ_2 and ϵ_3 are small, the two related results match consistently. With the increases of ϵ_1, ϵ_2, and ϵ_3, the discrepancy between them gradually increases.

Owing to the approximations made in the study it is expected that the approximate analytical solutions are valid for small parameters ϵ_1, ϵ_2 and ϵ_3. This is confirmed by the excellent agreement between the analytical and numerical results.

A numerical search for $2(N/M)\pi$ instabilities was conducted for the cases studied analytically in §4.3.3. Insignificant instabilities were found in all cases. The

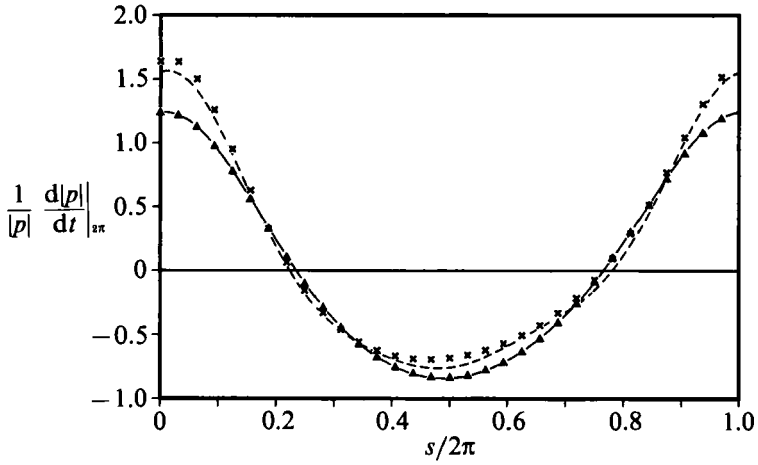

FIGURE 5. $(1/|p|)(\mathrm{d}|p|/\mathrm{d}t)|_{2\pi}$ is shown as a function of s. Symbols are the same as figure 4.

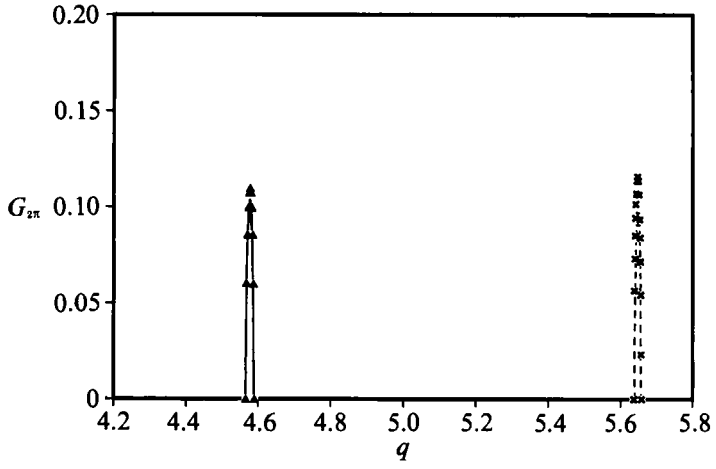

FIGURE 6. $G_{2\pi}$ is shown as a function of q for: $\epsilon_1 = 0.05$, $\epsilon_2 = 0.03$ and $\epsilon_3 = 0.0005$ (——, analytical; △, numerical); and $\epsilon_1 = 0.05$, $\epsilon_2 = 0.05$ and $\epsilon_3 = 0.01$ (– – –, analytical; ×, numerical).

magnitudes of q_b and G_{max} for $\epsilon_3 = 0.01$ are $O(10^{-7})$ when $\epsilon_1 = \epsilon_2 = 0.1$, and $O(10^{-6})$ when $\epsilon_1 = \epsilon_2 = 0.2$. In both cases q_b and G_{max} are much less than $O(\epsilon_1^2 \epsilon_2^4 T^{-2})$, and thus are consistent with the approximate results. These magnitudes are comparable to the numerical errors tolerated in the computation, and cannot definitely be considered as instability.

5.2. *Numerical results*

To investigate the influence of the scale parameters ϵ_1, ϵ_2 and ϵ_3 on the conventional sideband and $2N\pi$ instabilities, we show their global resonant growth G as functions of q and ϵ_2 in figures 7(*a*)–7(*c*) for a fixed $\epsilon_3 = 0.01$, and $\epsilon_1 = 0.10$, 0.20 and 0.30, respectively. They are also shown as functions of q and $\epsilon_3^{-\frac{1}{4}}$ in figure 8 for $\epsilon_1 = 0.10$ and $\epsilon_2 = 0.10$. Since the instabilities are symmetric with respect to $q = 0$ and q is limited to $O(1)$ for the validity of the perturbation method, we only plot instabilities for $0 \leqslant q \leqslant 6$.

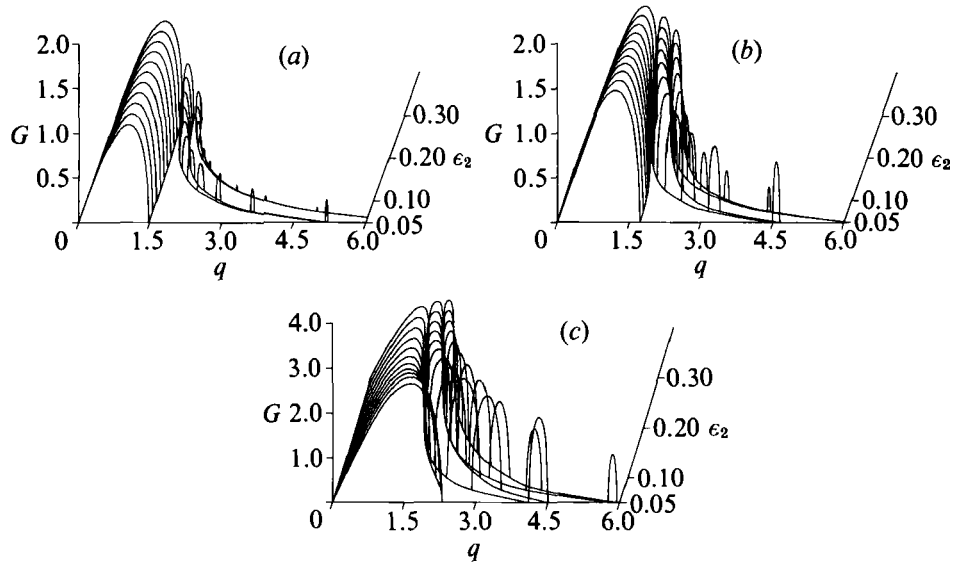

FIGURE 7. The global resonant growth G and bandwidth q_b are shown as functions of q and ϵ_2 for $\epsilon_3 = 0.01$, and (*a*) $\epsilon_1 = 0.10$; (*b*) $\epsilon_1 = 0.20$; (*c*) $\epsilon_1 = 0.30$.

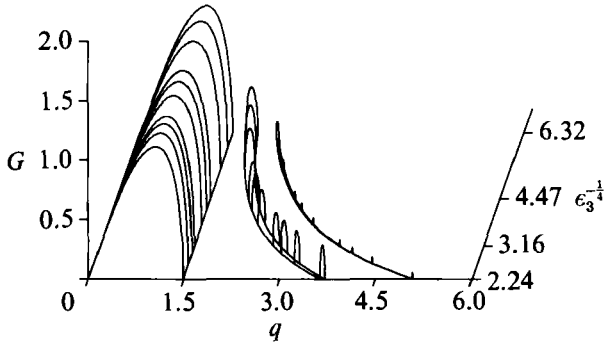

FIGURE 8. G and q_b are shown as functions of q and $\epsilon_3^{-\frac{1}{4}}$ for $\epsilon_1 = \epsilon_2 = 0.1$.

The conventional sideband instability region is in the neighbourhood of $q = 0$. The 2π and 4π instability regions are located at large q. When ϵ_1 and ϵ_2 are small and ϵ_3 is relatively large ($\epsilon_3 = 0.01$), the conventional sideband instability is dominant, with a large resonant bandwidth, q_b, of approximately $\sqrt{2}$, and G_{max} slightly larger than one. Both are much greater than the corresponding parameters of the $2N\pi$ instabilities. Of the $2N\pi$ instabilities, the 2π instability is the strongest, with G_{max} and q_b of $O(\epsilon_1)$. The resonant regions are separated by wide stable regions.

For large ϵ_1 values, q_b and G_{max} for the conventional sideband instability increase slightly, while those for the $2N\pi$ instabilities increase rapidly and their resonant regions shift slightly towards $q = 0$. When $\epsilon_1 = 0.20$ and 0.30 (figures 7*b*, *c*), q_b and G_{max} of the 2π and 4π instabilities are comparable to those of the conventional sideband instability.

As ϵ_2 increases (as shown in figure 7*a*–*c*) and/or ϵ_3 decreases (as shown in figure 8), or q_b and G_{max} of the conventional sideband instability both decrease. The decrease is too slow to be observed clearly in figures 7 and 8. To display this trend, in

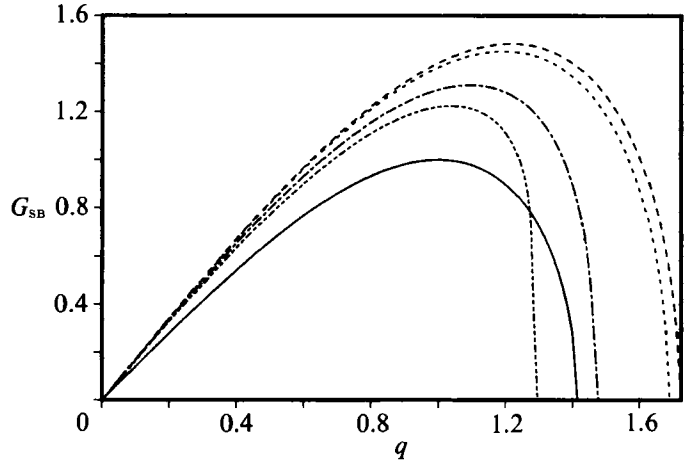

FIGURE 9. The normalized global sideband resonant growth G_{SB} is shown as a function of q for $\epsilon_1 = 0.20$, $\epsilon_3 = 0.01$ and $\epsilon_2 = 0.05$ (————), 0.1 (– – –), 0.2 (————————) and 0.3 (————— – – – ———). The corresponding result (——) for an equivalent wave train travelling on otherwise calm water is also given for comparison.

figure 9 we show G for the sideband instability as a function of q for fixed $\epsilon_1 = 0.20$, $\epsilon_3 = 0.01$ and ϵ_2 increasing in the range 0.05–0.30. The slight decrease of G_{max} and q_b for the conventional sideband instability with respect to ϵ_2 is consistent with the analytical result in §4.3.1. It should be noted that a similar phenomenon has been observed, with the resonant bandwidth of the normalized perturbation wavenumber and the growth rate decreasing with the increase of the wave steepness, in the study of the stability of a wave train on otherwise calm water (Yuen & Lake, 1982), but the causes of the seemingly similar phenomena are quite different. In the absence of the long wave, the decreases in normalized resonant growth rate and the bandwidth of the normalized perturbation wavenumber are due to the contribution from the higher-order terms, whereas in our study, the related higher-order terms are truncated and the decreases result from the modulation by the long wave.

With the increase of ϵ_2 or decrease of ϵ_3, the resonant bandwidth q_b and the maximum global growth G_{max} of the $2N\pi$ instabilities notably increase. Their resonant regions move towards the conventional sideband resonant region.

These changes of G and q_b of the sideband and $2N\pi$ instabilities with respect to ϵ_1, ϵ_2 and ϵ_3 are qualitatively consistent with the approximate solutions presented in §§4.3.1 and 4.3.2. For relatively large ϵ_1 and ϵ_2 ($0.2 \sim 0.3$), or very small $\epsilon_3(10^{-4})$, the three resonant regions are so close that they seem to merge. Detailed numerical evidence reveals that there always exists a stable region between two adjacent resonant regions in the range of our numerical computation. This is accompanied by a decrease in the bandwidths of the 2π and 4π instabilities, with their bandwidths being smaller at $\epsilon_2 = 0.3$ than those at $\epsilon_2 = 0.20$ when ϵ_1 is relatively large (0.2–0.3). This behaviour of q_b for the $2N\pi$ instabilities is not predicted by the approximate solutions of §4.3.2.

The $2N\pi$ instabilities for $N \geqslant 3$ are not plotted in figures 7 and 8, because their occurrence at large q may lead to $\tilde{K} \approx 1.0$ which violates the assumptions of the perturbation approach.

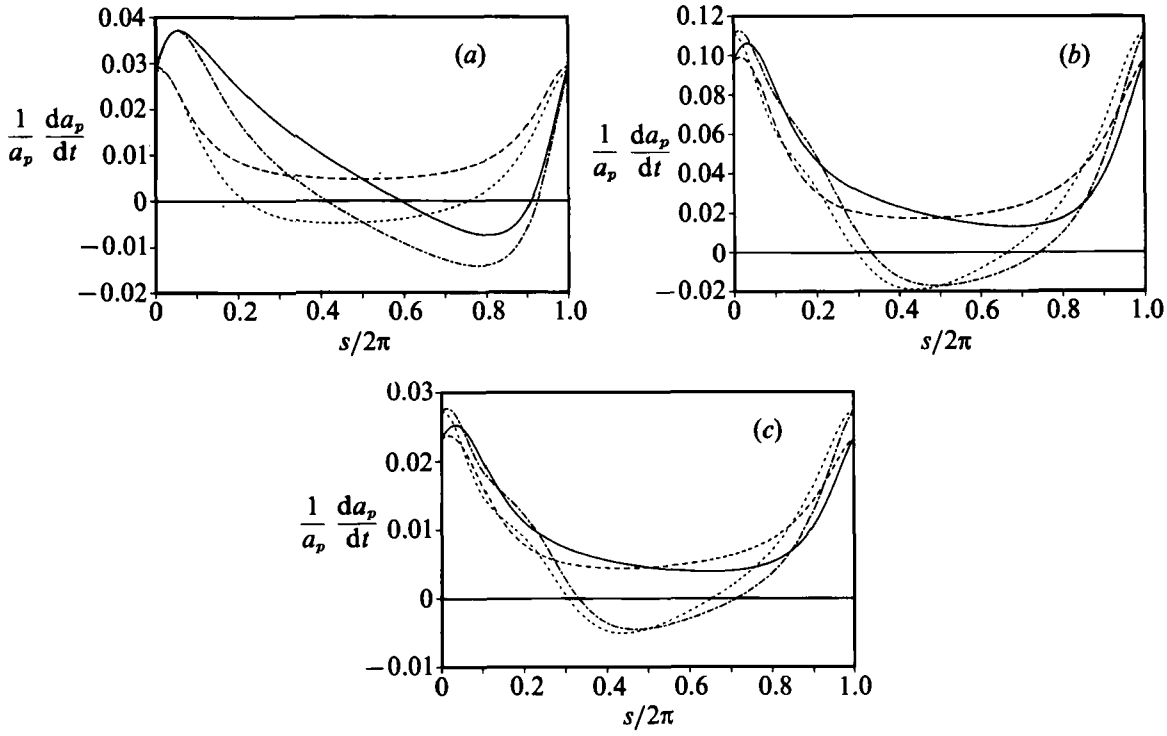

FIGURE 10. The total growth rate of disturbances is shown as a function of s for $\epsilon_1 = 0.20$, and (a) $\epsilon_2 = 0.10$, $\epsilon_3 = 0.01$; (b) $\epsilon_2 = 0.20$, $\epsilon_3 = 0.01$; (c) $\epsilon_2 = 0.01$, $\epsilon_3 = 0.0004$. For reference, the corresponding resonant growth rates are also given; sideband disturbances: ——, total growth rate; — — —, resonant growth rate. 2π instability disturbances: — · — · —, total growth rate; – – –, resonant growth rate.

6. Effect of modulation on the growth rate of disturbances

In addition to their resonant growth, the sideband disturbances travelling with the short-wave train along the long wave are also modulated by the long wave. Therefore, we should consider the effect of modulation on the rate of change of the disturbance amplitude.

According to (2.8a), (2.1) and (2.9), the amplitude of disturbances measured in the (x, z)-plane is given by

$$a_p = |p|\frac{|b|\,\sigma}{g_1 H_0}. \tag{6.1}$$

Using the assumption that the amplitude profile of the short-wave train is steady relative to the long-wave surface, the change of the disturbance amplitude may be explicitly expressed as a function of the position on the long wave,

$$\frac{1}{a_p}\frac{da_p}{dt} = \frac{1}{|p|}\frac{d|p|}{dt} + \frac{1}{a_a^{(11)} k_0}\left(R_c H_0^2 + \frac{\sigma}{2k}\right)\frac{\partial a_a^{(11)}}{\partial s}. \tag{6.2}$$

The first term on the right-hand side of (6.2) accounts for the resonant growth rate, and the second term represents the modulation rate.

The total growth rate of disturbances displaying a maximum global resonant growth in the conventional sideband or 2π resonant regions is shown as a function of the position on the long wave in figure 10. For comparison, the corresponding resonant growth rate is also plotted. The difference between the total growth rate

and the resonant growth rate is hence the modulation rate. In order to show how fast the disturbances vary along the long wave, the total growth rate and the resonant growth rate have not been normalized by the maximum resonant growth rate of an equivalent wave train. They are only normalized by σ_0 as implied in the normalization of time. The influence of the scale parameters ϵ_1, ϵ_2 and ϵ_3 on the total growth rate of the disturbances are explored in these figures. In figures 10(*a*) and 10(*b*), ϵ_1 and ϵ_3 are fixed. For smaller ϵ_2 ($= 0.1$), the total growth rates of the sideband disturbances, $(1/|a_p|)(\mathrm{d}|a_p|/\mathrm{d}t)|_{\mathrm{SB}}$ and the 2π instability disturbance, $(1/|a_p|)(\mathrm{d}|a_p|/\mathrm{d}t)|_{2\pi}$ are negative along most of the rear face of the long wave. For larger ϵ_2 ($= 0.20$), both are close to their corresponding resonant growth rates, being slightly greater (smaller) on the forward (rear) face of the long wave. That is, when ϵ_2 is smaller than ϵ_1, the modulation rate plays an important role in the total growth rate. With the increase of ϵ_2, its role in the total diminishes.

In figures 10(*a*) and 10(*c*), ϵ_1 and ϵ_2 are fixed. For a relatively large ϵ_3 ($= 0.01$, figure 10*a*), the effect of the modulation on the total growth of disturbances is significant. With a small ϵ_3 ($= 0.0004$, figure 10*c*), the modulation becomes unimportant. This is because when the wavelength ratio decreases, the modulation rate decreases approximately in proportion to the square root of the wavelength ratio, while the resonant growth rate is virtually unchanged.

Consideration of the total growth rate of the disturbance amplitude implies that short waves are more unstable on the forward face of the long wave. This may contribute to short-wave breaking on the forward face of the long wave.

7. Implications for wave energy transfer

We have studied the instability of a short-wave train riding on a periodic long wave. Some of the assumptions (e.g. irrotational flow, free-surface boundary conditions) may have limited validity for real ocean waves. However, the $2N\pi$ instability may have important implications for nonlinear energy transfer in short wind waves.

With the $2N\pi$ instability, the resonant bandwidth of the perturbation wavenumber is wider (though not continuous) than that for a short wave riding on calm water. The quartet resonance in a broadband wave train is known to be related to the sideband resonance (Longuet-Higgins 1976, hereinafter referred to as LH; Janssen 1983). In the light of the $2N\pi$ sideband instability, corresponding new types of resonances are expected to exist in a broadband short-wave train riding on a long wave. Following the analogy between the sideband instability and quartet resonance, we discuss below the resonance condition and the wave-action transfer rate of these new resonances.

By comparison with the 2π instability, the corresponding conditions for the resonant quintet interaction in a broadband short-wave train modulated by a long wave are expected to be

$$\boldsymbol{k}_1+\boldsymbol{k}_4+K_d=\boldsymbol{k}_2+\boldsymbol{k}_3, \tag{7.1}$$

$$\sigma_1+\sigma_4+\Omega_d=\sigma_2+\sigma_3, \tag{7.2}$$

where $K_d < |\boldsymbol{k}_1| \leqslant |\boldsymbol{k}_2| \leqslant |\boldsymbol{k}_3| \leqslant |\boldsymbol{k}_4|$ and long-wave propagation in the positive x-direction are assumed. Following LH, we examine whether or not (7.1) and (7.2) are the linear resonance condition for this new quintet resonance and determine the leading order of the wave-action transfer rate. Instead of using coordinates

translating with the wave train, we obtain the wave-action transfer rate in fixed coordinates,

$$\frac{dC_1}{dt} = \mathrm{Re}\left\{ \sum_{2,3,4} \int_0^t dt' \left[(C_4+C_1)\,C_2\,C_3 - (C_2+C_3)\,C_1\,C_4\right] e^{i[(\sigma_2+\sigma_3-\sigma_1-\sigma_4)(t'-t)-K_d x]} \right.$$
$$\left. \times\, \delta(\boldsymbol{k}_2+\boldsymbol{k}_3-\boldsymbol{k}_1-\boldsymbol{k}_4-K_d)\right\}, \quad (7.3)$$

where $C_l (l = 1\text{–}4)$ is the action of wave l. With the exception of an additional long wavenumber K_d in the delta function and consequently an extra term, $-iK_d x$, in the phase function, equation (7.3) resembles equation (4.8) of LH. If the long wavelength is much larger than those of short waves, at the leading order the modulated wave actions can be approximated by

$$C_l = \bar{C}_l\,[1 + 2\epsilon_1 \cos(K_d x - \Omega_d t)], \quad (7.4)$$

where the overbar denotes the time or space average. Substituting (7.4) into (7.3), the change rate of the averaged wave action with respect to time due to the quintet resonance is given by

$$\frac{d\bar{C}_1}{dt} = 3\epsilon_1 \pi \sum_{2,3,4} \left[(\bar{C}_4+\bar{C}_1)\,\bar{C}_2\,\bar{C}_3 - (\bar{C}_2+\bar{C}_3)\,\bar{C}_1\,\bar{C}_4\right]$$
$$\delta(\sigma_2+\sigma_3-\sigma_1-\sigma_4-\Omega_d)\,\delta(\boldsymbol{k}_2+\boldsymbol{k}_3-\boldsymbol{k}_1-\boldsymbol{k}_4-K_d). \quad (7.5)$$

The delta functions in (7.5) confirm the resonance conditions suggested by (7.1) and (7.2). The leading order of the wave-action transfer rate of the quintet resonance is $3\epsilon_1$ times as large as that of the conventional quartet resonance given by LH. Hence, the former may be comparable to the latter if the long wave is significant, say $\epsilon_1 = 0.1\text{–}0.2$.

The $2N\pi$ instability of a narrowband short-wave train riding on a long wave indicates a new type of resonant energy transfer mechanism in a broadband short-wave train riding on a long wave. A more complete study of this new resonance and its implications for wind–wave, wave–wave interactions in the ocean will be carried out in the future.

We thank an anonymous referee for comments leading to a clarification of the equilibration argument of §3.1. This work was supported by NSF Engineering Research Centers under Grant No. CDR-8721512 and Texas Advanced Technology Research Program under Grant No. 14509 to J.Z., and by NSF OCE-8614889 to W.K.M.

Appendix A. The Derivation of (4.7) and (4.8)

The effective gravitational acceleration g_1 is defined in ZM as

$$g_1 = \frac{g\cos\theta}{H_0} + C^2 H_0 \left.\frac{\partial H}{\partial n}\right|_{n=0}, \quad (A\,1)$$

where θ is the local slope of the long-wave surface and is given by

$$\theta = \tan^{-1}(\eta_s / x_s). \quad (A\,2)$$

Using (A 2) and recalling that K_d is normalized to unity and $C^2 \approx g(1+\epsilon_1^2)/K_d$, (A 1) is simplified to

$$g_1 = g\left[x_s\Big|_{n=0} + (1+\epsilon_1^2)\,H_0 \left.\frac{\partial H}{\partial n}\right|_{n=0}\right] + O(\epsilon_1^4)\,g, \quad (A\,3)$$

where H is given by (4.3). For ease of computation, it is not normalized with respect to H_{00} here. The derivative of g_1 with respect to s is given by

$$\frac{\partial g_1}{\partial s} = g\left[x_{ss}|_{n=0} + (1+\epsilon_1^2)\left(H_0 \frac{\partial^2 H}{\partial n \partial s}\bigg|_{n=0} + \frac{\partial H_0}{\partial s}\frac{\partial H}{\partial n}\bigg|_{n=0}\right)\right], \tag{A 4}$$

where, using (4.2), (4.3) and (4.4),

$$x_{ss}|_{n=0} = -\epsilon_1 \sin s - 4\epsilon_1^2 \sin 2s + O(\epsilon_1^3), \tag{A 5}$$

$$H_0 \frac{\partial^2 H}{\partial s \partial n}\bigg|_{n=0} = H_0^4(\epsilon_1 \sin s + 6.5\epsilon_1^2 \sin 2s) + O(\epsilon_1^3), \tag{A 6}$$

$$\frac{\partial H_0}{\partial s}\frac{\partial H}{\partial n}\bigg|_{n=0} = -H_0^6 \tfrac{1}{2}\epsilon_1^2 \sin 2s + O(\epsilon_1^3). \tag{A 7}$$

Substituting (A 5)–(A 7) into (A 4), and recalling that $g_1 = g[1+O(\epsilon_1^2)]$, we obtain equation (4.7):

$$\frac{1}{g_1}\frac{\partial g_1}{\partial s} = O(\epsilon_1^3).$$

According to the linear dispersion relation (4.5), we have

$$\frac{2}{\sigma}\frac{\partial \sigma}{\partial s} = \frac{2}{H_0}\frac{\partial H_0}{\partial s} + \frac{1}{k}\frac{\partial k}{\partial s} + \frac{1}{g_1}\frac{\partial g_1}{\partial s}. \tag{A 8}$$

According to the phase conservation and (4.6), we have

$$\frac{\partial \sigma}{\partial s} = -H_0^2 Ck\left[\frac{2}{H_0}\frac{\partial H_0}{\partial s} + \frac{1}{k}\frac{\partial k}{\partial s}\right]. \tag{A 9}$$

Substituting (A 9) into (A 8) it is found that

$$\frac{2}{\sigma}\frac{\partial \sigma}{\partial s}\left[1 + \frac{g_1}{2R_c\sigma}\right] = \frac{1}{g_1}\frac{\partial g_1}{\partial s}. \tag{A 10}$$

Since $R_c^{-1} \sim O(\epsilon_3^{\frac{1}{3}})$, we find equation (4.8):

$$\frac{1}{\sigma}\frac{\partial \sigma}{\partial s} = \frac{1}{2g_1}\frac{\partial g_1}{\partial s}[1 + O(\epsilon_3^{\frac{1}{3}})] \sim O(\epsilon_1^3).$$

Appendix B. Benjamin–Feir instability of equivalent waves

The wavenumber and steepness of a modulated short wave at the intersection of the long-wave surface and calm water level is given approximately by

$$k = a^{(11)}k = 1 + 2\epsilon_1 - \epsilon_1^2. \tag{B 1}$$

The Benjamin–Feir instability of the equivalent wave on calm water can be straightforwardly determined. The maximum resonant growth is given by

$$\frac{1}{|p|}\frac{\mathrm{d}|p|}{\mathrm{d}t} = \tfrac{1}{2}\epsilon_2^2(a^{(11)}k)^2, \tag{B 2}$$

when

$$q_{\max} = a^{(11)}k. \tag{B 3}$$

After the time required for the short wave to travel one long wavelength in the moving coordinates, the resonant growth is equal to

$$G = \tfrac{1}{2}\epsilon_2^2 T^{-1}(1 + 6\epsilon_1 + 10\epsilon_1^2). \tag{B 4}$$

The approximations for resonant growth rate, global resonant growth and perturbation wavenumber given in §4 are normalized by (B 2)–(B 4), respectively.

In accordance with the approximate solution, the numerical results depicted in §5 are also expressed in terms of ratio to $(1/|p|)(\mathrm{d}|p|/\mathrm{d}t)$, G and $q_{\max}$, respectively, except that the wavenumber and steepness of the equivalent wave and the time for a short wave to travel one long wavelength are obtained numerically.

REFERENCES

Benjamin, T. B. & Feir, J. E. 1967 The disintegration of wave trains on deep water. *J. Fluid Mech.* **27**, 417–430.

Drazin, P. G. & Reid, W. H. 1981 *Hydrodynamic Stability*. Cambridge University Press.

Dysthe, K. B. 1979 Note on a modification to the nonlinear Schroedinger equation for application to deep water waves. *Proc. R. Soc. Lond.* A **369**, 105–114.

Hasselmann, K. 1962 On the nonlinear energy transfer in a gravity-wave spectrum. Part 1. General theory. *J. Fluid Mech.* **12**, 481–500.

Henyey, F. S., Creamer, D. B., Dysthe, K. B., Schult, R. L. & Wright, J. A. 1988 The energy and action of small waves riding on large waves. *J. Fluid Mech.* **189**, 443–462.

Iooss, G. & Joseph, D. D. 1980 *Elementary Stability and Bifurcation Theory*. Springer.

Janssen, P. A. E. M. 1983 On a fourth-order envelope equation for deep-water waves. *J. Fluid Mech.* **126**, 1–11.

Longuet-Higgins, M. S. 1976 On the nonlinear transfer of energy in the peak of a gravity-wave spectrum: a simplified model. *Proc. R. Soc. Lond.* A **347**, 311–328 (referred to herein as LH).

Longuet-Higgins, M. S. 1987 The propagation of short surface waves on longer gravity waves. *J. Fluid Mech.* **177**, 293–306.

Mackay, R. S. & Saffman, P. G. 1986 Stability of water waves. *Proc. R. Soc. Lond.* A **406**, 115–125.

Magnus, W. & Winkler, S. 1966 *Hills Equation*. Wiley-Interscience.

McLean, J. W., Ma, Y. C., Martin, D. V., Saffman, P. G. & Yuen, H. C. 1981 Three-dimensional instability of finite-amplitude water waves. *Phys. Rev. Lett.* **46**, 817–820.

Phillips, O. M. 1960 On the dynamics of unsteady gravity waves of finite amplitude. Part 1. *J. Fluid Mech.* **11**, 143–155.

Phillips, O. M. 1981 The dispersion of short wavelets in the presence of a dominant long wave. *J. Fluid Mech.* **107**, 465–485.

Whitham, G. B. 1965 A general approach to linear and nonlinear dispersive waves using a Lagrangian. *J. Fluid Mech.* **22**, 273–283.

Whitham, G. B. 1974 *Linear and nonlinear waves*. Wiley.

Yuen, H. C. & Lake, B. M. 1982 Nonlinear dynamics of deep-water gravity waves. *Adv. Appl. Mech.* **22**, 67–229.

Zakharov, V. E. 1968 Stability of periodic waves of finite-amplitude on the surface of a deep fluid. *J. Appl. Mech. Tech. Phys.* **9**, 190–194.

Zhang, J. 1990 Nonlinear interaction between short and long waves. *NSF OTRC Rep.* 6/90-A-3-100.

Zhang, J. 1991 Fourth-order Lagrangian of a short wave riding on a long wave. *Phys. Fluids*, In press.

Zhang, J. & Melville, W. K. 1990 Evolution of weakly nonlinear short waves riding on long gravity waves. *J. Fluid Mech.* **214**, 321–346 (referred to herein as ZM).